Constraining the Volatility Distribution and Gas-Particle Partitioning of Combustion Aerosols Using Isothermal Dilution and Thermodenuder Measurements

ANDREW P. GRIESHOP,[†] MARISSA A. MIRACOLO, NEIL M. DONAHUE, AND ALLEN L. ROBINSON*

Center for Atmospheric Particle Studies, Carnegie Mellon University, Pittsburgh Pennsylvania 15213

Received November 17, 2008. Revised manuscript received March 2, 2009. Accepted March 8, 2009.

The gas-particle partitioning of primary organic aerosol (POA) emissions from a diesel engine and the combustion of hard- and soft-woods in a stove was investigated by isothermally diluting them in a smog chamber or by passing them through a thermodenuder and measuring the extent of evaporation. The experiments were conducted at atmospherically relevant conditions: low concentrations and small temperature perturbations. The partitioning of the POA emissions from both sources varied continuously with changing concentration and temperature. Although the POA emissions are semivolatile, they do not completely evaporate at typical atmospheric conditions. The overall partitioning characteristics of diesel and wood smoke POA are similar, with wood smoke being somewhat less volatile than the diesel exhaust. The gas-particle partitioning of aerosols formed from flash-vaporized engine lubricating oil was also studied; diesel POA is somewhat more volatile than the oil aerosol. The experimental data from the dilution- and thermodenuder-based techniques were fit using absorptive partitioning theory to derive a volatility distribution of the POA emissions from each source. These distributions are suitable for use in chemical transport models that simulate POA concentrations.

Introduction

Combustion sources emit a complex mixture of organics that span a wide range of volatility (*1, 2*). The amount of primary organic aerosol (POA) depends on the gas-particle partitioning of this mixture (*3*); however, POA has historically been treated as nonvolatile by chemical transport models and emission inventories (*4*). The implicit assumptions are that (1) gas-particle partitioning measured using a dilution sampler at modest dilution is representative over the full range of atmospheric conditions, and (2) semivolatile material contributes only a small fraction of the total POA. Neither of these assumptions is valid. A large fraction of the POA can evaporate when emissions are isothermally diluted from the high-concentration conditions typically found inside dilution samplers to more atmospherically relevant concentrations (*3, 5, 6*). Thermodenuder measurements have also shown substantial evaporation with modest increases in temperature (*7*−*9*).

Gas-particle partitioning of atmospheric organics is thought to be an absorptive process. It therefore depends on temperature, the concentrations of the emissions and sorptive material, and the volatility distribution of the emissions (*10, 11*). Partitioning behavior can be modeled using a set of lumped species; this is a standard approach for secondary organic aerosol (SOA) (*12*) and has recently been used for POA (*3, 6, 8*). This semiempirical approach relies on fitting experimental data; however, the existing fits or volatility distributions for POA are not well-constrained across the entire range of atmospheric conditions (*3, 6*).

The goal of this paper is to investigate gas-particle partitioning of POA across a wide range of atmospherically relevant conditions by systematically diluting or heating emissions from important sources. We apply absorptive partitioning theory to the data to derive volatility distributions for the emissions expressed using the volatility-basis-set (VBS) framework (*10*).

Materials and Methods

We investigated the effects of temperature and concentration on the gas-particle partitioning of POA. Separate experiments considered emissions from a diesel engine, wood stove, and flash-vaporized lubricating oil. Emissions from soft- and hardwood fires were sampled from a small wood stove (Cabela's Sheepherder's Packer Stove); Grieshop et al. (*8*) provides details on the stove operation and fuels. The diesel engine was a Yanmar L-A series air-cooled 1-cylinder 4-cycle 6.6 HP engine connected to a generator. The engine-generator system operates at constant speed; these experiments were conducted with emissions from the engine operating at low load (∼25%) on fuel purchased from a local service station. Unburned lubricating oil is thought to be the dominant component of POA in diesel emissions (*2, 13*). Lubricating oil aerosol was created by flash vaporizing used SAE 10W-30 oil at 425 °C. The oil had been used for 130 h in a Caterpillar D6H 3306 diesel engine. Initial mass-weighted median diameters ranged from 90 to 130 nm for the diesel particles, 100 to 190 nm for the wood smoke particles, and 150 to 200 nm for the lubricating oil particles.

There are differences, such as the compression ratio and fuel injection technology, between our diesel engine and state-of-the-art diesel engines. All of these factors influence emissions. However, the AMS mass spectra presented in the Supporting Information indicate that the emissions from our engine are similar to those from other diesel engines. Our engine may also be more similar to older, higher-emitting, in-use engines that disproportionately contribute to emission inventories.

Biomass-burning is also a highly variable source. Our measurements of POA from fuel-wood burned in a wood stove are most representative of biomass smoke produced by residential heating fires. However, many of the properties of our emissions (combustion efficiencies, OC/EC ratios, etc) are similar to emissions from other types of biomass fires such as open burns and wildfires (*8*).

Emissions from each source were injected into the Carnegie Mellon University smog chamber via a heated stainless-steel inlet maintained at 250−350 °C to minimize thermophoretic losses of particles and condensation of semivolatile compounds in the inlet. The smog chamber is

* Corresponding author phone: (412) 263−3657; fax: (412) 268−3348; e-mail: alr@andrew.cmu.edu.

[†] Currently at Institute for Resources, Environment and Sustainability, University of British Columbia, Vancouver, British Columbia, Canada, V6T1Z4.

10.1021/es8032378 CCC: $40.75

a 12 m^3 temperature-controlled Teflon film bag. Before each experiment, the chamber was cleaned and then filled with HEPA- and activated-carbon-filtered air (*8*). Upon entering the chamber the aerosols were rapidly diluted and cooled to 22 ± 2 °C; initial concentrations ranged from 70 to 1300 $\mu g\ m^{-3}$.

After injection the aerosols were allowed to equilibrate for about an hour and then the gas-particle partitioning was perturbed by either isothermally diluting the contents of the chamber using the approach of Grieshop et al. (*14*) or by continuously drawing a sample from the chamber through a thermodenuder (TD) system. Most of the TD measurements were made with the system of An et al. (*15*); however, some experiments used an Aerodyne TD (*16*). To investigate the dynamics of evaporation, the ambient temperature centerline residence time (CLRT) in the heated section of the An et al. (*15*) TD was varied from 3 to 47 s. The CLRT of the Aerodyne TD was 3 s. When both TD systems were operated at the same residence time, the measurements of the two systems agreed to within experimental uncertainty. The TD data were corrected for particle losses based on the particle number penetration efficiency. These corrections are discussed in the Supporting Information.

The extent of evaporation was measured with a scanning mobility particle sizer (SMPS, TSI 3936) and an Aerodyne quadrapole aerosol mass spectrometer (AMS) (*17*). The AMS data were corrected for the contribution from gas-phase CO_2 at m/z 44 and then analyzed using the fragmentation table of Allan et al. (*18*). In TD experiments, AMS and SMPS measurements were alternated every 15−30 min between the TD and a bypass line maintained at 25 °C.

To estimate the extent of evaporation, we calculated the volume fraction remaining (VFR) from the SMPS data and the OA mass fraction remaining (OA MFR) from the AMS data:

$$\mathrm{VFR} = \frac{d_{\mathrm{m}}^3}{d_{\mathrm{m,o}}^3} \quad \mathrm{OAMFR} = \frac{C_{\mathrm{TD}}}{C_{\mathrm{bypass}}} \tag{1}$$

where $d_{m,o}$ and d_m are the SMPS volume-median-mobility diameters and C_{bypass} and C_{TD} are the AMS organic aerosol mass concentrations on the bypass line or downstream of the TD, respectively, VFR was similarly used to quantity particle evaporation in dilution experiments with $d_{m,o}$ and d_m indicating diameter before and after dilution. We also calculated the VFR using a range of particle size percentiles (10th, 25th, median, 75th, etc.), which indicated that the entire size distribution shrank uniformly.

The VFR analysis assumes that the particles are spherical with constant density, assumptions that are not necessarily valid for combustion generated particles. Data from the SMPS and AMS were combined to estimate particle density and the particle fractal dimension (*19*). The estimated fractal dimension for the particles emitted by this engine at low load and for the wood smoke emissions was approximately 3, indicating that the particles were essentially spherical. At low load, emissions from this engine are predominantly organic not elemental carbon (*5*), so any fractal soot is likely heavily coated by adsorbed organics. The wood smoke particles were also predominantly organic carbon (*8*).

Volatility Basis-Set Fitting. The volatility-basis-set (VBS) framework (*10*) was used to parametrize the measured partitioning behavior. Briefly, the VBS is a set of lumped species with effective saturation concentrations (C^*) spaced by factors of 10 at ambient temperature (298 K). Absorptive partitioning theory expresses the particle fraction (X_p) as a function of the concentration of organic aerosol (C_{OA}):

$$X_{\mathrm{p}} = \sum_{i=1}^{n} f_i \left(1 + \frac{C_i^*}{C_{\mathrm{OA}}}\right)^{-1} \tag{2}$$

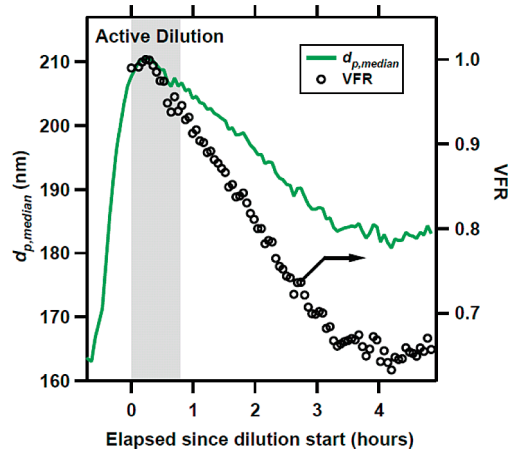

FIGURE 1. Time series of volume-median-mobility diameter and volume fraction remaining (VFR, see eq 1) measured during an in-chamber dilution experiment conducted with lubricating oil aerosol. The shaded area indicates when the chamber was actively diluted with HEPA- and activated-carbon-filtered air.

where f_i represents the mass fraction of the total semivolatile material found in the C_i^* volatility bin. This set of f_i's is the volatility distribution of the emissions. Here we fit the partitioning data using a 9-bin VBS ranging from 10^{-2} to 10^6 $\mu g\ m^{-3}$ at 298 K; the fitting procedure is described in the Supporting Information.

Results

Dilution Measurements. In-chamber dilution experiments were performed with diesel exhaust and lubricating oil aerosols. Figure 1 shows time series of data from a typical experiment. The initial aerosol concentration was 1300 $\mu g\ m^{-3}$ based on the SMPS measurements and assuming unit density. After allowing the aerosol to equilibrate for about an hour, the chamber was actively diluted for a 45-min period. Dilution reduces the concentration of suspended particles and vapors inside the chamber.

To illustrate the changes in the particle size distribution due to this dilution, time series of the volume-median-mobility diameter and VFR are plotted in Figure 1. Before dilution, the median particle diameter increased from about 160 to 210 nm mainly due to coagulation (the experiments were conducted in the dark). The growth in particle diameter stopped after 15 min of active dilution and then the particles began to shrink. They continued to shrink for about 2.5 h after active dilution was stopped, ultimately reaching an equilibrium median diameter of about 165 nm. In control experiments (aerosol injection but no in-chamber dilution) the particles continue to grow by coagulation at an ever-slowing rate over a period of several hours until they reach a constant median size.

Shrinking particles are an unambiguous indication of evaporation due to dilution (AMS nonrefractory mass and SMPS volume have a strong linear correlation, ruling out density changes). Approximately 20% of the particle mass evaporated when the wall-loss corrected organic aerosol concentration inside the chamber was reduced from 1300 $\mu g\ m^{-3}$ to 450 $\mu g\ m^{-3}$. As discussed below, wall loss complicates quantitative analysis of the data, but the results clearly indicate that dilution caused substantial evaporation of particle mass.

All in-chamber dilution experiments showed the same behavior as Figure 1. Dilution caused substantial evaporation, but the evaporation rate was slow. In every experiment, it took an hour or more after the active dilution phase for the aerosol to reach equilibrium. This is much slower than expected, especially relative to the rapid condensation of

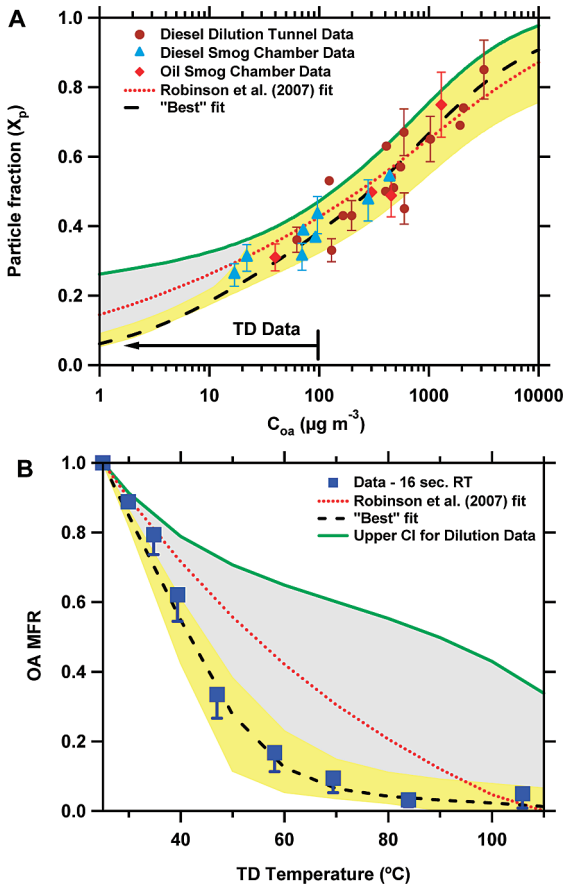

FIGURE 2. Compilation of experimental data and VBS fits for diesel and lubricating oil primary organic aerosol. (a) Particle fraction (X_p, fraction of semivolatile organic material found in condensed phase) versus organic aerosol concentration (C_{OA}). The "dilution tunnel data" are from refs *5 and 6*; other data are from the in-chamber dilution experiments described in this manuscript. Arrow indicates concentration regime investigated with the TD. (b) Thermogram of organic aerosol mass fraction remaining (MFR, see eq 1) for lubricating oil measured at a TD residence time of 16 s. As described in the text, the gray-plus-yellow shaded region indicates confidence interval of fits of dilution data; yellow area indicates confidence interval of fits to dilution and thermodenuder data. Error bars in (a) indicate experimental uncertainty on selected data points. The TD data in (b) have been corrected for particle loss; the uncorrected data are shown by the error bars in (b).

lubricating oil vapor after its injection into the chamber. Using the dynamic equation for particle evaporation (*20*), we investigated the kinetics of the evaporation. The average particle shrinkage rate during the second half of the active dilution period shown in Figure 1 is consistent with an effective uptake coefficient of order 0.001 to 0.01 (a value of 1 is commonly assumed). The evaporation rate observed here is much slower than that of single-component aerosols (*20*), but similar to SOA formed from α-pinene ozonolysis (*14*). The reason for the slow evaporation of complex mixtures is not known. Particles lost to the chamber walls are unlikely to be the cause of the slow evaporation observed here; any delay in evaporation of wall-bound particles would tend to depress vapor concentrations and thus increase evaporation rates.

Figure 2a presents a partitioning plot that displays all of the in-chamber isothermal dilution data and previously published measurements made with dilution samplers for diesel POA (*5, 6*). Following partitioning theory (eq 2), the particle fraction (X_p) is plotted as a function of C_{OA}. For the in-chamber dilution measurements, the X_p values are referenced to our previously published partitioning measurements made with dilution samplers at high concentrations (*5, 6*). We assigned an initial X_p value (before dilution) based on the X_p values of the quartz-filter dilution-sampler measurements at a similar C_{OA}. The postdilution X_p values were then calculated by scaling the initial X_p value by the measured VFR.

For the in-chamber dilution experiments, C_{OA} is the wall-loss corrected SMPS mass concentration assuming a density of 1 g cm^{-3}. This approach assumes that all condensed-phase mass, both in suspension and that which has been deposited to the walls, participates in gas-particle partitioning, and that condensed-phase material on the chamber walls evaporates at the same rate as that in suspension. Data from SOA experiments support this assumption (*14, 21*). The mass lost to the walls was calculated assuming a first-order wall-loss rate and then scaled using the measured VFR of the suspended particles to account for evaporation (*14*). In these experiments, the evaporated mass tends to be small relative to that lost to the walls.

Figure 2a shows that some of the new partitioning data overlaps the existing data ($C_{OA} > 100\ \mu g\ m^{-3}$). Over this range, the relative amount of evaporation measured by the in-chamber dilution technique is very consistent with the dilution-sampler data, even though the two data sets are based on very different experimental techniques.

Figure 2a indicates that the new data extend the partitioning curve down to a C_{OA} value of 20 μg m^{-3}. The entire data set reveals a continuous change in POA partitioning from an X_p of 0.85 at C_{OA} of 10 000 μg m^{-3} to around 0.25 at 20 μg m^{-3}. The new dilution data also provide no evidence for a large nonvolatile component of the *organic* emissions, which is consistent with the diesel POA emissions being made up of a complex mixture of species more or less evenly distributed across a wide range of volatility (*1, 2*). However, the dilution measurements do not cover the entire atmospherically relevant range of C_{OA} because particle losses to the chamber walls make direct measurement of partitioning at very low C_{OA} difficult. Although the data clearly demonstrate that POA is semivolatile, the wood smoke and diesel emissions do contain a core of nonvolatile material that is not organic such as elemental carbon.

Thermodenuder Measurements. Thermodenuder (TD) measurements were used to further investigate partitioning, especially at low values of C_{OA} and X_p. Figure 3a shows a thermogram for engine lubricating oil particles at an initial chamber concentration of about 70 μg m^{-3}. A thermogram is a plot of OA MFR versus TD temperature. Figure 3a shows MFR data for two TD residence times: 3 and 16 s.

The thermograms in Figure 3a illustrate two important points. First, the OA MFR depends on residence time. This means that the aerosol does not necessarily reach equilibrium in the heated section of the TD (*15*). Measurements at longer residence suggest that the aerosol has reached equilibrium at a CLRT of about 20 s (see Figure S.3 in the Supporting Information). Uncertainty regarding equilibration in the TD means that data collected at short residence times only provide an *upper bound* for the POA volatility. Equilibration times in the TD are much shorter than in dilution experiments because the driving potential for temperature-driven evaporation in the TD is substantially higher than that for isothermal dilution in the smog chamber.

The second major conclusion from Figure 3a is that lubricating oil aerosol is quite volatile. For example, at even the shortest residence time, more than half of the particle mass evaporated at a TD temperature of 60 °C. The slope of the OA MFR data near 25 °C provides an estimate of the sensitivity of the POA partitioning to small perturbations in temperature. This slope was −2% °C^{-1} for the 16 s data, indicating that the gas-particle partitioning of lubricating oil

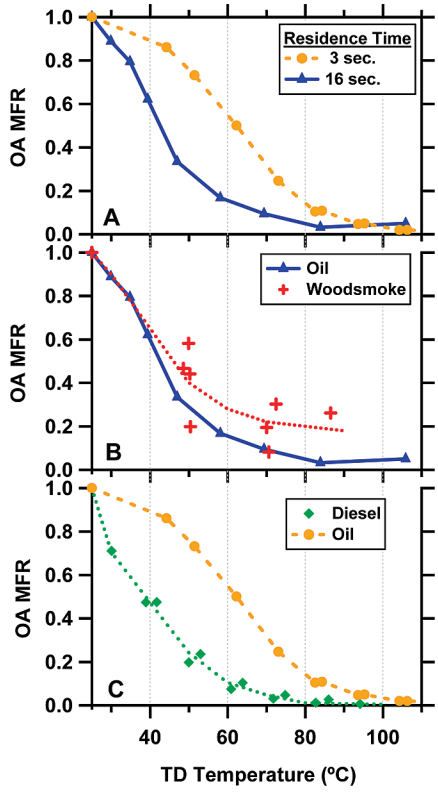

FIGURE 3. Thermograms of organic aerosol mass fraction remaining (OA MFR, see eq 1). (a) Lubricating oil aerosol at different thermodenuder residence times, (b) wood smoke and lubricating oil at a thermodenuder residence time of 16 s and (c) lubricating oil and diesel particulate matter at a thermodenuder residence time of 3 s. Curves are intended to guide the eye. The scatter in the wood smoke data reflects experiment-to-experiment variability (*8*).

aerosol varies substantially with small, atmospherically relevant changes in temperature.

Although the substantial evaporation of lubricating oil aerosol at temperatures less than 100 °C may seem surprising given that this is lower than typical oil temperatures in an operating engine, one cannot simply make comparisons based on temperature because phase-partitioning also depends on concentration. We investigated oil aerosol at atmospherically relevant concentrations (10s of $\mu g\,m^{-3}$) which are many orders of magnitude lower than those in an engine. Our motor oil aerosols are also somewhat more volatile than the original motor oil because the flash vaporizer is not 100% efficient (see Figure S.1 in the Supporting Information).

Figure 3 also presents thermograms for wood smoke and diesel POA. The wood smoke and diesel TD measurements were only made at residence times of 16 and 3 s, respectively. Therefore, the lubricating-oil data are used as a reference point for comparing volatility. The wood-smoke data are from Grieshop et al. (*8*); the scatter is experiment-to-experiment variability. Much less variability was observed with the diesel POA and lubricating oil aerosol (the diesel engine was always operated at the same load). The initial C_{OA} (pre-TD) for both wood smoke and diesel was about 100 $\mu g\,m^{-3}$.

Figure 3b shows that somewhat higher temperatures were required to evaporate the wood smoke POA than the lubricating oil particles. Therefore, wood smoke has more material in the lower C^* bins than motor oil. At 25 °C, the sensitivity of wood smoke POA to temperature changes is about the same as that of motor oil, $-2\%\ °C^{-1}$.

Figure 3c indicates that the diesel POA is more volatile than lubricating oil. For example, at 25 °C, the sensitivity of the diesel POA is $-6\%\ °C^{-1}$ versus $-1\%\ °C^{-1}$ for motor oil aerosol at the same residence time (3 s). This difference is somewhat surprising since lubricating oil is thought to be dominant component of diesel POA (*2, 13*). A possible explanation is that diesel POA is a mixture of fuel and oil (*22*). However, the AMS mass spectra of our diesel POA are most similar to reference spectra for lubricating oil, but notably less similar to reference diesel fuel spectra (see Figure S.2 in the Supporting Information). This suggests that diesel POA may consist of the more volatile fractions of the lubricating oil. Finally, smaller particles evaporate more rapidly than larger particles (*23*). Since the diesel particles were about half the size of the lubricating oil aerosol, the differences shown in Figure 3c could largely be due to evaporation kinetics which are most significant for the 3 s residence time data.

Other researchers have performed volatility tandem differential mobility analyzer measurements of diesel particulate matter (*13, 24*). These measurements also show substantial particle evaporation, but at higher temperatures than those reported here. However, the previous studies used very short residence times. Since the extent of evaporation depends strongly on both temperature and residence time, it is difficult to quantitatively compare our data with the previous work.

Volatility Distributions

The gas-particle partitioning data were fit using the VBS framework to determine volatility distributions for wood smoke and diesel POA. Figures 2 and 4 plot the fits for diesel and wood smoke POA, respectively. The fits are shown as lines with confidence intervals indicated by shaded areas.

The fitting was a two-step process. First, the dilution data were fit 100 times using a nonlinear fitting algorithm coupled to a Monte Carlo scheme to quantify the uncertainty of the fit (see the Supporting Information). The result is 100 different volatility distributions for each source. The diesel fits included the previously published dilution sampler data (*5, 6*) and the new in-chamber dilution data for both diesel and lubricating oil. Initial wood smoke fits were based only on previously published dilution sampler data (*5, 6*). The median R^2 value for the 100 diesel fits was 0.72 and 0.94 for the 100 wood smoke fits.

Confidence intervals were then defined using the fifth and 95th percentiles of the envelope of the 100 fits in the X_p versus C_{OA} space. These confidence intervals are indicated by the shaded regions in Figures 2a and 4a. Figure 4a shows that the fits of the wood-smoke data diverge at C_{OA} values less than about 100 $\mu g\ m^{-3}$ because of the lack of low-concentration data (*6*). In comparison, Figure 2a shows that the diesel fits are better constrained over the entire C_{OA} range due to our new in-chamber dilution data. In both cases, if the remaining POA was non-volatile then minimum observed X_p would be the actual minimum. Therefore, the upper confidence intervals (green lines) level off near the minimum observed X_p.

In step two of the fitting process, the TD are used to further constrain the fits in the lowest volatility bins. First, the OA MFR as a function of temperature was calculated for all 100 VBS fits derived in step 1 using equilibrium partitioning theory (eq 2). The temperature-dependence of C^* was calculated using the Clausius−Clapeyron equation and the enthalpies of vaporization (ΔH_{vap}) listed in Supporting Information Table S.1. These ΔH_{vap} values are based on data for large saturated species commonly found in primary emissions (*1*); they dictate that a 20−25 °C increase in temperature increases C^* by about a factor of 10. Figure 3 indicates that most of the OA entering the TD ($\sim$ 100 $\mu g\ m^{-3}$) evaporated when its temperature was increased by 50 °C; therefore, most of this material must be in the 100 and/or 10 $\mu g\ m^{-3}$ C^* bins.

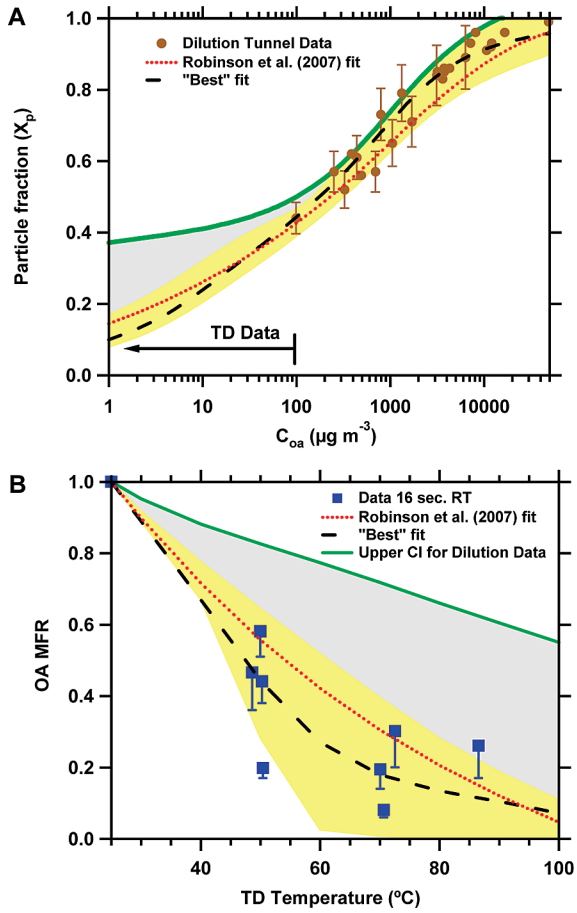

FIGURE 4. Compilation of experimental data and VBS fits for wood smoke primary organic aerosol. (a) Particle fraction (X_p, fraction of semivolatile organic material found in condensed phase) versus organic aerosol concentration (C_{OA}) data from (*5, 6*). (b) Thermogram of organic aerosol mass fraction remaining (MFR, see eq 2) measured at 16 s of residence time. As described in the text, the gray-plus-yellow shaded region indicates confidence interval of fits of dilution data; yellow area indicates confidence interval of fits dilution and thermodenuder data. Error bars in (a) indicate experimental uncertainty (on selected data points). The TD data in (b) have been corrected for particle loss; the uncorrected data are shown by the error bars in (b).

To illustrate how the TD data provide an additional constraint, the OA MFR values calculated using all of the fits from step 1 are shown as the gray-plus-yellow shaded regions in Figures 2b and 4b. The TD data clearly fall near the lower (most volatile) end of this range. Consequently, we eliminated fits from step 1 that fell outside of the uncertainty bounds of the TD data to obtain the narrower yellow confidence interval for each source. This reveals that only the most-volatile distributions from step 1 match the TD measurements. The TD data thus complement the dilution data by constraining the lower volatility (lower C_{OA}) range.

The TD data also highlight that the gas-particle partitioning of POA varies across the entire range of atmospherically relevant conditions. This conclusion holds whether or not the aerosol has reached equilibrium in the TD. If it has not, then this conclusion only becomes stronger because incompletely evaporated particles would give MFR values *above* the equilibrium value.

Table 1 lists the nine-bin volatility distributions (set of f_i's in eq 2) that best describe the combined data sets (volatility distributions for the confidence intervals are provided in Supporting Information Table S.2). These distributions are expressed as the mass fraction of material collected on a quartz filter with a dilution sampler operated at low-dilution-ratio/high-concentration conditions. Therefore they represent the volatility distribution of the POA emissions in existing emission inventories. These fits are compared to the experimental data in Figures 2 and 4.

TABLE 1. Volatility Distributions for Diesel and Wood Smoke Primary Organic Aerosol

C^* at 298 K (μg m^{-3})	wood smoke[a]	diesel[a,b]
10^{-2}	0.05	0.01
10^{-1}	0	0.01
1	0.05	0.04
10	0.25	0.21
100	0.15	0.18
1000	0.45	0.45
10^4	0	0.1
10^5	0.05	0
10^6	0	0

[a] Mass fraction of organics collected on a quartz filter at low-dilution-ratio/high-concentration conditions using a dilution sampler. [b] The TD data required assigning a small amount of diesel emissions (1%) to in an even lower volatility bin (10^{-3} μg m^{-3}) than is contained in our 9-bin VBS. This material has been listed in the 10^{-2} μg m^{-3} C^* bin because material with C^* values of 10^{-3} and 10^{-2} μg m^{-3} essentially behave the same over the atmospherically relevant range of temperatures and C_{OA} values.

The distributions notably do not contain much material in the very low volatility bins; for example, the three lowest C^* bins contain less than 10% of the mass. This was required to make the fits consistent with the TD data. It means that only a small fraction of the organic material in the emissions from either source can be considered nonvolatile. The distributions also contain essentially no material in the very high volatility (IVOC) bins, e.g. 10^6 μg m^{-3}; however, this does *not* imply that there are no emissions in this volatility range, only that emissions in this range are poorly collected by quartz filters. Comprehensive characterization of IVOC emissions requires sampling with sorbents.

The volatility distributions listed in Table 1 are not unique (*25*). For example, other statistically acceptable fits shift some material among neighboring bins but do not alter any of our substantive conclusions. The fits also depend on assumed parameters such as ΔH_{vap} values. Changing these values requires refitting the data to derive new volatility distributions. The distributions listed in Table 1 in combination with the assumed ΔH_{vap} provide a self-consistent set of parameters that reproduce the observed changes in partitioning.

Chromatography data provide a check on the volatility distributions. The best-fit distributions for both sources assign about 80% of the emissions as measured by a quartz filter to C^* bins of 10, 100, and 1000 μg m^{-3}. These bins nominally contain material with volatilities between *n*-octacosane (C_{28}), which has a C^* of about 5 μg m^{-3}, and *n*-nonadecane (C_{19}), which has a C^* of about 5000 μg m^{-3}, according to vapor-pressure data compiled in SciFinder Scholar (accessible with subscription at https://scifinder.cas.org). Carbon-number based chromatography of diesel particulate matter indicates that more than 60% of the organics collected on a quartz filter elutes between these two *n*-alkanes (*1*).

Figures 2 and 4 also compare the new fits to the volatility distribution previously derived by Robinson et al. (*3*) dotted (red curves) using a subset of diesel dilution sampler data. Robinson et al. (*3*) used this fit to represent gas-particle partitioning of all primary emissions in a chemical transport model. The Robinson et al. (*3*) distribution provides a reasonable representation of both the diesel and wood-smoke data.

Discussion

The results presented here illustrate the semivolatile character of POA emitted by two important source classes: wood combustion and diesel engines. We believe this is a defining characteristic of POA and must be accounted for in models. The volatility distributions listed in Table 1 can be combined with existing nonvolatile POA emission factors measured with dilution samplers at high concentrations to derive volatility based emissions for chemical transport modeling (*3*).

Our data indicate that the gas-particle partitioning of POA varies with changing atmospheric conditions. The sensitivity of the POA to changes in temperature ranged from −1 to −6% $°C^{-1}$ at 25 °C, which is comparable to published data for SOA formed in smog chambers (*26*). This implies that diurnal and seasonal temperature changes may drive large changes in POA partitioning. The sensitivity of the wood-smoke and the diesel POA to changes in C_{OA} is −3% $(\mu g\ m^{-3})^{-1}$ at a C_{OA} of 1 $\mu g\ m^{-3}$ and −0.9% $(\mu g\ m^{-3})^{-1}$ at a C_{OA} of 10 $\mu g\ m^{-3}$.

Although POA emissions are semivolatile, they do not completely evaporate at typical atmospheric conditions. The majority of the material in the 0.01, 0.1, and 1 $\mu g\ m^{-3}$ C^* bins will always partition into the condensed phase. Both the wood smoke and diesel emissions also contain some nonvolatile material that is not organic, such as elemental carbon.

By combining data from three complementary techniques—dilution sampler measurements, in-chamber dilution experiments, and thermodenuder measurements—we have derived a volatility distribution that describes the gas-particle partitioning of POA emissions over a wide range of atmospheric conditions. The TD data were especially useful at constraining the fits in the lowest volatility bins.

Acknowledgments

We thank Byong-Hyoek Lee for his assistance with the CMU thermodenuder and Jesse Kroll for his assistance with the Aerodyne thermodenuder. Funding was provided by the EPA STAR program through the National Center for Environmental Research (NCER) under grant R833748, by the U.S. Department of Energy through the National Energy Technology Laboratory under Grant No. 41817M203841817M2000, and by the U.S. Department of Defense Strategic Environmental Research and Development Program (SERDP). The views, opinions, and/or findings contained in this paper are those of the authors and should not be construed as an official position of any of the funding agencies.

Supporting Information Available

Additional information, tables, figures, and references. This material is available free of charge via the Internet at http://pubs.acs.org.

Literature Cited

(1) Hildemann, L. M.; Mazurek, M. A.; Cass, G. R.; Simoneit, B. R. T. Quantitative characterization of urban sources of organic aerosol by high-resolution gas-chromatography. *Environ. Sci. Technol.* **1991**, *25* (7), 1311–1325.

(2) Schauer, J. J.; Kleeman, M. J.; Cass, G. R.; Simoneit, B. R. T. Measurement of emissions from air pollution sources. 2. C-1 through C-30 organic compounds from medium duty diesel trucks. *Environ. Sci. Technol.* **1999**, *33* (10), 1578–1587.

(3) Robinson, A. L.; Donahue, N. M.; Shrivastava, M. K.; Weitkamp, E. A.; Sage, A. M.; Grieshop, A. P.; Lane, T. E.; Pierce, J. R.; Pandis, S. N. Rethinking organic aerosols: semivolatile emissions and photochemical aging. *Science* **2007**, *315*, 1259–1262.

(4) Donahue, N. M.; Robinson, A. L.; Pandis, S. N. Atmospheric organic particulate matter: From smoke to secondary organic aerosol. *Atmos. Environ.* **2009**, *43* (1), 94–106.

(5) Lipsky, E. M.; Robinson, A. L. Effects of dilution on fine particle mass and partitioning of semivolatile organics in diesel exhaust and wood smoke. *Environ. Sci. Technol.* **2006**, *40* (1), 155–162.

(6) Shrivastava, M. K.; Lipsky, E. M.; Stanier, C. O.; Robinson, A. L. Modeling semivolatile organic aerosol mass emissions from combustion systems. *Environ. Sci. Technol.* **2006**, *40* (8), 2671–2677.

(7) Huffman, J. A.; Docherty, K. S.; Aiken, A. C.; Cubison, M. J.; Ulbrich, I. M.; DeCarlo, P. F.; Sueper, D.; Jayne, J. T.; Worsnop, D. R.; Ziemann, P. J.; et al. , Chemically-resolved aerosol volatility measurements from two megacity field studies. *Atmos. Chem. Phys. Discuss.* **2009**, *9*, 2645–2697.

(8) Grieshop, A. P.; Logue, J. M.; Donahue, N. M.; Robinson, A. L. Laboratory investigation of photochemical oxidation of organic aerosol from wood fires 1: measurement and simulation of organic aerosol evolution. *Atmos. Chem. Phys.* **2009**, *9*, 1263–1277.

(9) Kuhn, T.; Biswas, S.; Fine, P. M.; Geller, M.; Sioutas, C. Physical and chemical characteristics and volatility of PM in the proximity of a light-duty vehicle freeway. *Aerosol Sci. Technol.* **2005**, *39* (4), 347–357.

(10) Donahue, N. M.; Robinson, A. L.; Stanier, C. O.; Pandis, S. N. Coupled partitioning, dilution, and chemical aging of semivolatile organics. *Environ. Sci. Technol.* **2006**, *40* (8), 2635–2643.

(11) Pankow, J. F. An absorption-model of gas-particle partitioning of organic-compounds in the atmosphere. *Atmos. Environ.* **1994**, *28* (2), 185–188.

(12) Odum, J. R.; Hoffmann, T.; Bowman, F.; Collins, D.; Flagan, R. C.; Seinfeld, J. H. Gas/particle partitioning and secondary organic aerosol yields. *Environ. Sci. Technol.* **1996**, *30* (8), 2580–2585.

(13) Sakurai, H.; Tobias, H. J.; Park, K.; Zarling, D.; Docherty, S.; Kittelson, D. B.; McMurry, P. H.; Ziemann, P. J. On-line measurements of diesel nanoparticle composition and volatility. *Atmos. Environ.* **2003**, *37* (9−10), 1199–1210.

(14) Grieshop, A. P.; Donahue, N. M.; Robinson, A. L. Is the gas-particle partitioning in alpha-pinene secondary organic aerosol reversible? Geophys. Res. Lett. 2007, *34*, (L14810), DOI: 10.1029/2007GL029987.

(15) An, W. J.; Pathak, R. K.; Lee, B.; Pandis, S. N. Aerosol volatility measurement using an improved thermodenuder: Application to secondary organic aerosol. *J. Aerosol Sci.* **2007**, *38* (3), 305–314.

(16) Huffman, J. A.; Ziemann, P. J.; Jayne, J. T.; Worsnop, D. R.; Jimenez, J. L. Development and characterization of a fast-stepping/scanning thermodenuder for chemically-resolved aerosol volatility measurements. *Aerosol Sci. Technol.* **2008**, *42* (5), 395–407.

(17) Canagaratna, M. R.; Jayne, J. T.; Jimenez, J. L.; Allan, J. D.; Alfarra, M. R.; Zhang, Q.; Onasch, T. B.; Drewnick, F.; Coe, H.; Middlebrook, A.; et al. , Chemical and microphysical characterization of ambient aerosols with the aerodyne aerosol mass spectrometer. *Mass Spectrom. Rev.* **2007**, *26* (2), 185–222.

(18) Allan, J. D.; Delia, A. E.; Coe, H.; Bower, K. N.; Alfarra, M. R.; Jimenez, J. L.; Middlebrook, A. M.; Drewnick, F.; Onasch, T. B.; Canagaratna, M. R.; et al. , A generalised method for the extraction of chemically resolved mass spectra from aerodyne aerosol mass spectrometer data. *J. Aerosol Sci.* **2004**, *35* (7), 909–922.

(19) Slowik, J. G.; Stainken, K.; Davidovits, P.; Williams, L. R.; Jayne, J. T.; Kolb, C. E.; Worsnop, D. R.; Rudich, Y.; DeCarlo, P. F.; Jimenez, J. L. Particle morphology and density characterization by combined mobility and aerodynamic diameter measurements. Part 2: Application to combustion-generated soot aerosols as a function of fuel equivalence ratio. *Aerosol Sci. Technol.* **2004**, *38* (12), 1206–1222.

(20) Bilde, M.; Pandis, S. N. Evaporation rates and vapor pressures of individual aerosol species formed in the atmospheric oxidation of alpha- and beta-pinene. *Environ. Sci. Technol.* **2001**, *35* (16), 3344–3349.

(21) Weitkamp, E. A.; Sage, A. M.; Pierce, J. R.; Donahue, N. M.; Robinson, A. L. Organic aerosol formation from photochemical oxidation of diesel exhaust in a smog chamber. *Environ. Sci. Technol.* **2007**, *41* (20), 6969–6975.

(22) Kleeman, M. J.; Riddle, S. G.; Robert, M. A.; Jakober, C. A. Lubricating oil and fuel contributions to particulate matter emissions from light-duty gasoline and heavy-duty diesel vehicles. *Environ. Sci. Technol.* **2008**, *42* (1), 235–242.

(23) Faulhaber, A. E.; Thomas, B. M.; Jimenez, J. L.; Jayne, J. T.; Worsnop, D. R.; Ziemann, P. J. Characterization of a thermodenuder- particle beam mass spectrometer system for the study of organic aerosol volatility and composition. *Atmos. Meas. Tech.* **2009**, *2*, 15–31.

(24) Kwon, S. B.; Lee, K. W.; Saito, K.; Shinozaki, O.; Seto, T. Size-dependent volatility of diesel nanoparticles: Chassis dynamometer experiments. *Environ. Sci. Technol.* **2003**, *37* (9), 1794–1802.

(25) Stanier, C. O.; Donahue, N.; Pandis, S. N. Parameterization of secondary organic aerosol mass fractions from smog chamber data. *Atmos. Environ.* **2008**, *42* (10), 2276–2299.

(26) Stanier, C. O.; Pathak, R. K.; Pandis, S. Measurements of the volatility of aerosols from alpha-pinene ozonolysis. *Environ. Sci. Technol.* **2007**, *41* (8), 2756–2763.

ES8032378